TECHNICAL ARTICLE

Thermal Stress Measurement of a Double Ring Structure Using Digital Image Correlation Method

T.L. Jin, S.H. Lee*, and N.S. Goo

Smart Microsystem Research Laboratory, Department of Advanced Technology Fusion, Konkuk University, Seoul, South Korea

Keywords
Digital Image Correlation Method, Thermal Stresses, Thermal Analysis, Finite Element Method

Correspondence
N.S. Goo,
Smart Microsystem Research Laboratory,
Department of Advanced Technology Fusion,
Konkuk University,
Seoul, South Korea
Email: nsgoo@konkuk.ac.kr

*Present address: Agency for Defense Development, Deajeon, Korea.

Received: April 20, 2012;
accepted: August 19, 2013

doi:10.1007/s40799-016-0022-z

Abstract

Structures under a wide range of temperatures have been challenged by thermal problems. In order to assess the safety of structures in a thermal environment, thermal deformation and stress of structures should be determined by analysis and/or experimental method. This article presents a measurement method of the thermal deformation and stress of a double ring structure, which uses the digital image correlation method (DIC). The stress distribution of the double ring was obtained using a two-dimensional stress–strain relation. Efforts to remove measurement noise in the calculation of strain and stress are explained in detail. In order to verify the proposed measurement method, a finite element analysis of the double ring structure was performed using ABAQUS software. The results of DIC-based measurement and finite element analysis were found to be in good agreement.

Introduction

In a high speed flight, the surface temperature of supersonic and hypersonic aircrafts and spacecrafts exceeds 1000°C due to transient aerodynamic heating.[1] Therefore, thermal strain and thermal stress distributions of high temperature structures, as well as accurate temperature measurement, are important in designing aircraft structures and selecting suitable materials. In addition to aerospace applications, thermal strain and stress measurements are important in various engineering fields, such as jet engine and nuclear reactor.

Strain gages are commonly used to measure the deformation (strain) of a structure, especially thermal deformation. When strain gages are used in a high temperature condition, an inevitable error called thermal output occurs.[2] Thermal output occurs because of the resistance changes of the conductor in the strain gage due to temperature changes, and because of the difference in the coefficient of thermal expansion (CTE) between the strain gage and the structure to be measured. To eliminate thermal output, the strain gages attached on a low CTE material were used as the reference gages in the construction of a half/full bridge circuit. However, these gages had a limited operating temperature range and were not suitable for high temperature applications.

In addition to experiencing thermal output and temperature limitation, these gages were limited to point measurements and were difficult to apply to thin, flexible and small size structures. Several non-contact measurement methods without these weaknesses have been proposed: laser speckle correlation,[3] Moiré Interferometry,[4,5] electronic speckle pattern interferometry,[6] photoelastic-coating method,[7] and digital image correlation method (DIC).[8,9] In terms of the level of operational difficulty, price, quality of measurement area, and measurement result, the DIC is considered to be the most promising optical full-field measurement method.[10]

DIC is a typical non-contact optical deformation measurement method that has many applications, such as deformation test, dynamic deformation test, fracture mechanics test and thermal deformation test.[11–16] Noncontact deformation measurement

method plays an important role in measurements of biostructures, biomaterials, thin materials, films, and micro-level specimens, where sensors cannot be attached.[13] Horacio et al. investigated the hierarchical structures in seashells using *in situ* atomic force microscopy fracture experiments and the digital image correlation method.[17] Ha et al. measured the mechanical properties of a beetle hind wing using DIC, which would have been impossible to measure with a strain gage.[18]

Lyons et al.,[19] who first reported on thermal deformation measurement using the DIC (at least to the best of our knowledge), used the DIC to measure the deformation of an Inconel 718 alloy at temperatures up to 650°C. They mentioned that the image acquisition system could not obtain clear images of their specimen due to the radiation from the specimen over 650°C. Thompson et al. measured the thermal expansion of coating materials from room temperature up to 1050°C.[20] In recent researches, Pan et al. measured the thermal expansion coefficient of chromium–nickel stainless steel from room temperature up to 550°C.[10] The radiation from the test material was greater than that from a white light source, which was used in the image acquisition at a temperature of about 600°C. In 2010, Pan et al. used a narrow optical band-pass filter to solve the radiation problem and measured thermal expansions up to 1200°C.[21] Pan et al. also presented several papers on light source effect and the measurement of displacement fields and strain fields using DIC.[22]

In most of research, deformation, or strain, is the main physical variable. In other words, the deformation fields, or strain fields, from finite element analysis are compared with the experimental deformation or strain data. The stress can be determined from the strain by the theory of elasticity. This is a well-defined structural analysis procedure for a structure in a constant temperature environment. However, more attention is necessary to compare experimental deformation results with analysis deformation results in a variable temperature environment, as stress is related with not only strain but also temperature. An experimental method to determine the stress field from the strain field of a structure in a thermal environment needs to be developed, although this process of determining the stress field is well defined theoretically.

In this work, we adopted the digital image correlation method to measure the thermal deformation (strain) of a double ring structure consisting of an inner aluminum ring with high CTE and an outer titanium ring with low CTE. Furthermore, a method to postprocess the thermal stress from the thermal deformation (strain) measured by the DIC was developed. A double ring structure was heated in a chamber and the images of its surface were captured by a stereo-type camera. In addition, a finite element analysis of the double ring structure was performed using ABAQUS software. The deformation, strain and stress results from the DIC and the finite element analysis were compared. The method to reduce noise in the experimental stress field is explained in detail.

Basic Theory and Experimental Procedure

Digital image correlation method

DIC is a method used to calculate the deformation of a structure, using an image of the reference surface with an image of the deformed surface. The basic principle of the DIC is to track the same facet (subset) located in deformed images. Various correlation criteria have been published.[13] On the basis of the correlation criteria, the coordinates of the deformed points $\boldsymbol{P_v}$ can be obtained from the coordinates of the reference points $\boldsymbol{P_u}$:

$$\mathbf{P}_v = \mathbf{u} + \mathbf{F} \cdot \mathbf{P}_u \tag{1}$$

where the deformation gradient tensor $\boldsymbol{F}=\boldsymbol{RU}$ can be split to the rotation matrix $\boldsymbol{R}$ and the stretch tensor $\boldsymbol{U}$, and $\boldsymbol{u}$ is the rigid body translation. DIC can disregard rigid body translation and rotation when it calculates deformation. Two-dimensional DIC (2D-DIC) uses one digital camera and can measure in-plane deformation only. Three-dimensional DIC (3D-DIC) uses two digital cameras and can measure out-of-plane deformation as well as in-plane deformation.

Most of studies have used the 2D-DIC method, which uses one digital camera and can measure the in-plane deformation of a plate-shape specimen. However, 2D-DIC cannot eliminate the error from out-of-plane motion,[23] which appears in most mechanical experiments. Because 2D-DIC can measure only in-plane motion, a 3D-DIC should be used to measure out-of-plane motion.[24–27] Unlike the 2D-DIC, 3D-DIC uses a stereo-camera system to measure 3D images of the test surface. In this case, all the components of the displacements can be measured and the effects of out-of-plane rigid body motion on the in-plane deformation measurement can be easily eliminated. However, the two cameras have to be calibrated by a complex procedure.

Several factors should be considered in improving the quality of DIC measurements. A band-pass filter, circle polarized light filter and blue light emitting diode light can be used to improve image quality

significantly.[22] Aperture is also important for high quality image, particularly in 3D-DIC. A narrow aperture results in a sharp focus at the image plane because only highly collimated rays are admitted.[28] In 2D-DIC, the aperture is not very important because the camera is always set perpendicular to the object surface. In 3D-DIC, however, a proper aperture needs to be chosen for the two cameras to achieve enough depth of focus field and to obtain high resolution images because the two cameras are set obliquely to the specimen surface. In this experiment, the aperture was selected as 11 because the highest aperture of the lens was 22.

A double ring structure

This work aimed to measure full-field thermal deformation and stress. In order to verify the performance and accuracy of the full-field measurement method, a simple double ring structure was used. Figure 1(a) shows a double ring structure consisting of an inner aluminum ring with high CTE and an outer titanium ring with low CTE. The dimensions of the machined aluminum and titanium rings were measured at 25°C. The inner and outer diameters of the inner ring were 40.00 and 49.970 mm, respectively; the inner and outer diameters of the outer ring were 50.020 and 70.000 mm, respectively. The gap between the inner ring and outer ring was 25 μm in radius at 25°C. Figure 1(b) shows the real condition of two rings during experiment: the aluminum ring was supported by titanium ring and two rings were in contact at the bottom before experiment.

When the double ring structure was heated up in the heating chamber, the gap between the inner and outer ring decreased. Contact temperature is defined as the temperature at which the gap disappears:

$$T_{\text{contact}} = T_{\text{R}} + \frac{\text{GAP}}{\alpha_{\text{AL}} \times R_{\text{AL}} - \alpha_{\text{TI}} \times R_{\text{TI}}} \qquad (2)$$

where T_{contact} is the contact temperature of the inner and outer rings, T_{R} is the reference temperature, R_{AL} is the outer radius of the inner ring, R_{TI} is the inner radius of the outer ring, GAP is the initial gap between the inner ring and the outer ring, α_{AL} is the CTE of aluminum (22.5×10^{-6} m/m/°C, nominal value), and α_{TI} is the CTE of titanium (8.8×10^{-6} m/m/°C, nominal value). Assuming that CTE is not dependent on temperature during a temperature increase, the contact temperature was 98.08°C based on Eq. (2). Contact stress occurred between the two rings when the temperature was higher than the contact temperature.

Experimental setup

Figure 2 shows the experimental setup used to measure the thermal deformation of the double ring structure. The experimental setup consisted of the ARAMIS[29] system, a heating chamber (EC1A, Sun Electronic Systems, Inc., Titusville, FL) and a control computer. The ARAMIS system and the chamber were controlled by a computer using LabVIEW software (v8.6, NI, Austin, TX). The image acquisition system consisted of two cameras, which have 4 M pixel and 50 mm optical lens. The chamber can heat a specimen up to 320°C and also cool it down to −184°C using liquid nitrogen. An optical window was installed in the chamber wall. The cameras can take images through the window.

The glass, which was installed in the chamber window, was especially important for the measurement accuracy. The reflection on the glass surface could decrease the quality of images when the images were taken through the window. In order to eliminate the reflection effect, antireflection glass was used. The refraction also needs to be considered due to the image distortion. Two pieces of flat glass, whose thickness was 5 mm, were used to minimize the image distortion when the glass was heated.

Furthermore, over the past years, numerous experiments were performed to confirm the accuracy of the measurement system. Most of the experiments measure the CTE of material and thermal deformation of structures, such as aluminum, titanium, composite material, and microchips. With these measurement results, it can be concluded that the measurement system does not produce the significant errors due to the optical effects (reflection and refraction).

The image acquisition system was carefully calibrated to produce clear 3D images. First, the measurement field of view was set as $75 \times 75\ \text{mm}^2$, since the outer diameter of the outer ring was 70.000 mm. Second, the angle between the two cameras and the distance between the cameras and the specimen need to be determined based on the measurement field of view. The resolution of the camera was 2048×2048 pixels and the measurement field of view was set as $75 \times 75\ \text{mm}^2$, which means 1 pixel represented $37 \times 37\ \mu\text{m}^2$. Corresponding to the measurement field of view, specimen size, and camera resolution, the proper subset size was selected as 15 pixels.

The surface of the structure was specially treated to make a speckle pattern. Black and white paint was sprayed on the surface to make a high contrast random dot pattern. After camera calibration and speckle patterning, the specimen was placed in the chamber as shown in Figure 2(b). To improve

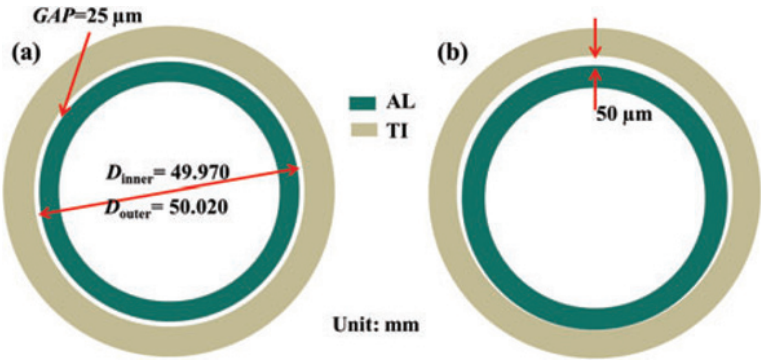

Figure 1 A double ring structure specimen. (a) Ideal condition and (b) real condition.

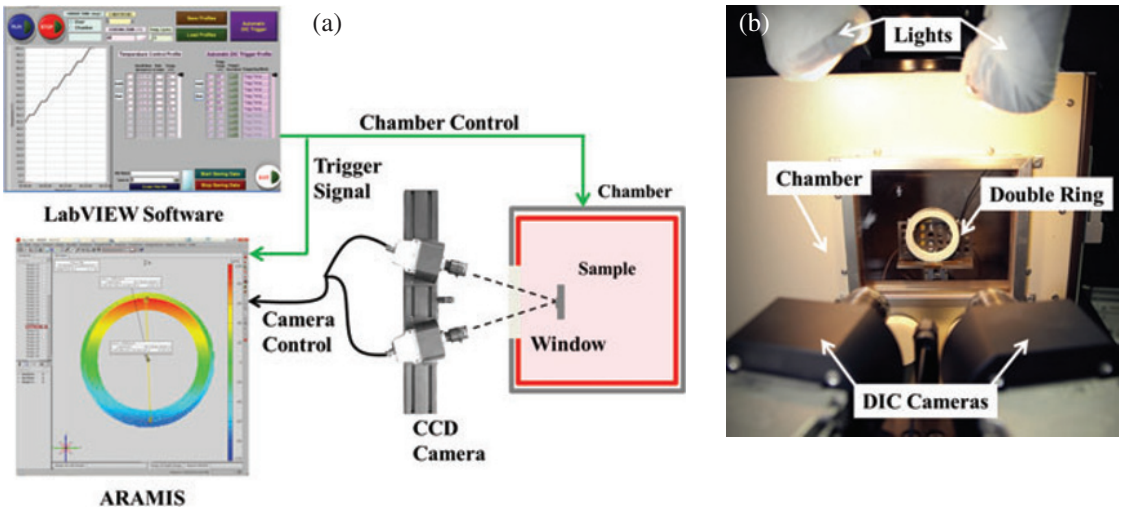

Figure 2 Experimental setup to measure the thermal deformation of a double ring structure using DIC.

image quality, aperture was selected as 11 in this experiment, as described in section Digital image correlation method. Shutter time was set to 0.1 second, which was the proper number in this experiment. Furthermore, additional light sources were used to overcome the insufficiency of light.

In the experiment, a reference image at 50°C was captured. Afterward, 30 images of the deformed specimen were consecutively recorded at temperature increments of 5°C up to 200°C. The double ring structure was heated from 50°C to 200°C at 5°C/min.

Finite element analysis

A finite element analysis was performed using the ABAQUS software to verify the accuracy of the experimental results. The finite element model had 30000 C3D8R (8-node three-dimensional element with reduced integration scheme) elements. Surface-to-surface contact elements were applied between the inner ring and the outer ring. Following the experimental condition, the bottom of the structure was in contact and the other area of the structure was separated in the model at the initial condition. To consider material nonlinearity, the temperature dependencies of CTE and elastic modulus were considered. As in the experiment, symmetric boundary conditions in two planes of symmetry and the fixed boundary condition along the edge were imposed on the model, as shown in Figure 3.

Accurate data on the mechanical properties of the structure were of great importance in the numerical analysis of a high temperature case. In this research, the aluminum and titanium used in this experiment were AL-2024-T351 and TI-6AL-4 V, respectively. The material properties were from metallic materials properties development and standardization (MMPDS)[30] and the values are listed in Table 1. To confirm the CTE of two materials, CTE measurement were performed and the measured CTE was very close to those in the MMPDS. Considering that the heating temperature was increased up to 200°C, the aluminum could not reach its tensile yield

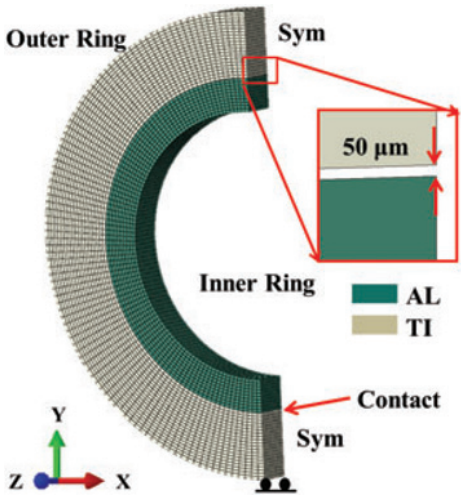

Figure 3 Double ring structure modeling.

Table 1 Elastic moduli and CTEs of aluminum and titanium[30]

	Aluminum (AL-2024-T351)		Titanium (TI-6AL-4 V)	
Temperature (°C)	CTE ($\times 10^{-6}$ m/m/°C)	Elastic modulus (GPa)	CTE ($\times 10^{-6}$ m/m/°C)	Elastic modulus (GPa)
50	22.68	76.69	8.87	114.11
100	23.22	75.24	9.05	110.62
150	23.58	72.35	9.22	107.12
200	23.94	67.29	9.36	103.63

strength, which was 131 MPa at 204°C. Therefore, plasticity of the materials was not considered in the analysis of the double ring.

Results and Discussions

Thermal deformation

In the experiment, rigid body translation and rotation were observed due to the mechanical noise in the heating chamber, the freely supported condition and thermal expansion of the platform. Therefore, 3D-DIC was necessary to carry out a precise experiment, and rigid body motion was eliminated from the 3D-DIC measurement result by using the movement correction algorithm.

Figure 4 shows the results of displacement u_y measured by the ARAMIS system and simulated by ABAQUS at 100 and 200°C. The maximum displacements of the inner ring measured by the ARAMIS system are 57.0 and 130.4 μm at 100 and 200°C, respectively. Similarly, the maximum displacements of the inner ring from the finite element analysis are 61.7 and 143.6 μm at 100 and 200°C, respectively. The comparison of the *y*-direction displacements between measurement and finite element analysis showed that the maximum displacements and the location of the maximum displacement of the inner ring were in good agreement between measurement and finite element analysis. Consequently, the measurement results were in good agreement with the analysis results.

The ARAMIS system can calculate the deformation of the structure using the reference image and also from images of the previous steps. Figure 5 shows u_y displacement contours for temperatures from 95 to 100°C and from 100 to 105°C. Figure 5(a) shows that the displacement of the inner ring is 1.4 μm greater than that of the outer ring, which means that the gap did not close at 100°C. Figure 5(b) shows that the displacements of both the inner and outer ring were 1.5 and 1.3 μm, which means that the gap had closed between 100 and 105°C. In other words, the rings contacted each other at about 100°C. According to Eq. 4, the contact temperature was 98°C as constant material properties were assumed in Eq. 4. This measurement result was in good agreement with theoretical result.

Changes in the diameters of the inner ring and outer ring were compared to confirm the accuracy of the measured displacements given by the ARAMIS system and by the analysis. The analysis and the experiment showed that the inner diameter of the outer ring was positively displaced by 98.4 and 94.8 μm (3.7% difference), respectively. Similarly, the analysis and the experiment showed that an outer diameter of the inner ring was positively displaced by 131.4 and 127.9 μm (2.7 % difference), respectively. The average changes in diameter of the inner ring and the outer ring were 2.01 and 2.52 μm after 100°C, respectively. The slope of the graph changes at around 100°C in Figure 6; this change indicates the contact between the inner ring and the outer ring.

Thermal strain and stress

Strain and stress fields are more important than displacement fields in material and structural stress analysis. However, large strain noise or strain error appeared at the contact region. The errors occurred if the reference and deformed facet was located at contact region, as shown in Figure 7. If a facet was located at the contact region, missing of speckle pattern in the facet produced big noise, or sometimes excessive deformation. Because of this phenomenon, the strain result shows abruptly different from that of the neighboring facets.

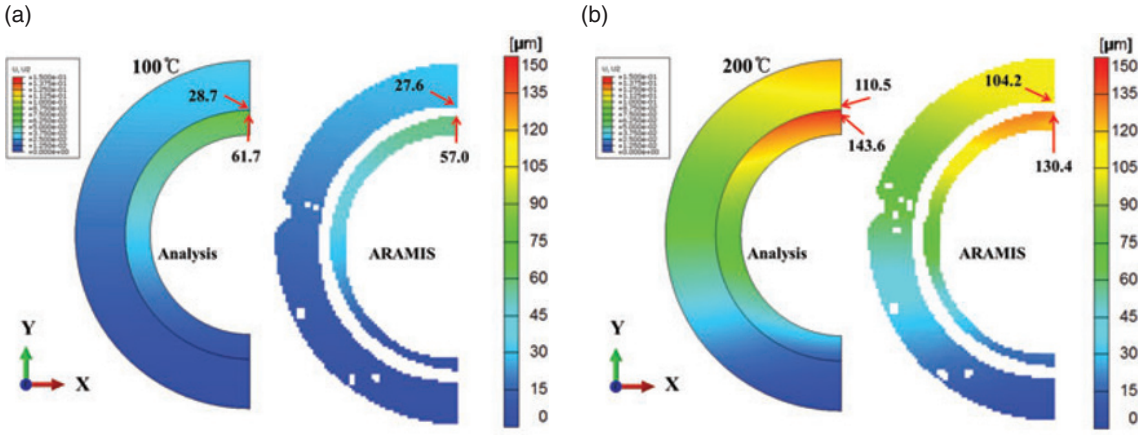

Figure 4 Comparisons of U_y displacement fields of double ring at (a) 100°C and (b) 200°C. Contours of analytical results and measurement results range from 0 to 0.15 mm (unit: μm).

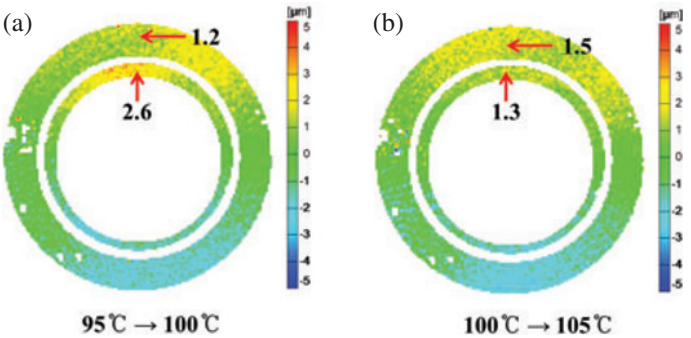

Figure 5 U_y displacments at 100°C and 105°C, respectively. (a) Displacements from 95°C to 100°C. (b) Displacements from 100°C to 105°C. (unit: μm).

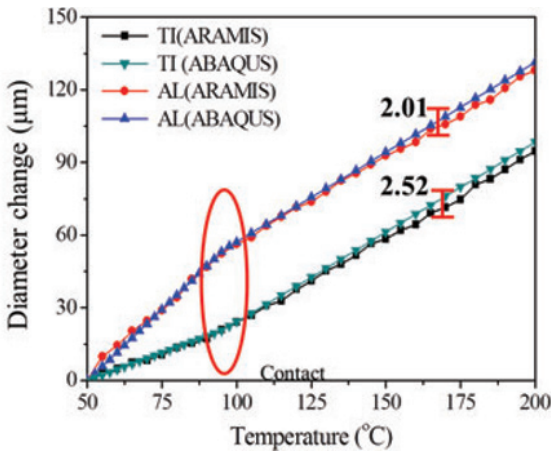

Figure 6 Changes in diameter and outer rings from analysis and ARAMIS system.

In order to reduce the error (noise) in the strain field, preprocessing and postprocessing procedures were performed in this work. First, an adequate subset size was selected based on measurement field, specimen size, and resolution of the cameras before DIC measurement. Considering all of the parameters, the proper subset size was selected as 15. Two kinds of postprocessing procedures were performed to reduce the noise in the strain and stress fields. In the first postprocessing procedure, the contact region of the rings was excluded from the calculation, because large errors occurred at the contact region of the test specimens and influenced neighboring facets when the average and median filters were applied. It is noted that this procedure did not cause discontinuity in displacement of two rings. In the second postprocessing procedure, a median filter, which is a kind of smoothing technique, was applied. It can effectively remove the noise that appears in the strain and stress fields measured by DIC. Figure 8 shows the original strain field and the strain field applied with postprocessing procedures. When Figure 8(c) is compared with Figure 8(a), it can be seen that the error and noise in the strain field were reduced significantly.

Figure 9 shows the comparisons of the total strain fields measured by the DIC and calculated by analysis at 200°C. The inner ring has a bigger deformation

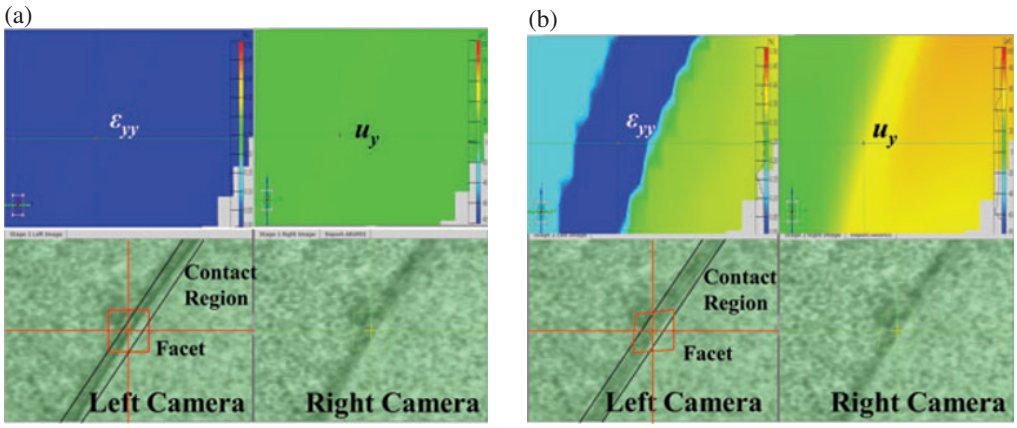

Figure 7 Left and right camera image and strain and displacement result at (a) reference stage and (b) deformed stage.

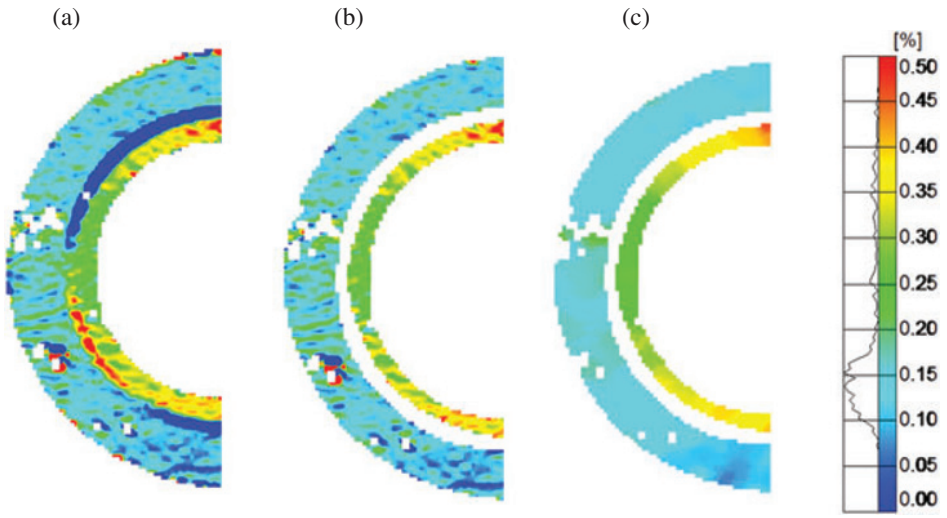

Figure 8 Y-direction total strain fields of the double ring measured at 200 °C by DIC. (a) Original strain fields from measurement, (b) strain field without the contact region of the two rings, (c) strain fields after application of median filter.

than the outer ring due to the initial gap between the inner and outer ring, as shown in Figure 9. The maximum strain ϵ_{xx} at the middle of the inner ring is 0.405% from the DIC and 0.402% from the analysis. Similarly, the maximum strain ϵ_{yy} at the top and bottom of the inner ring is 0.398% from the DIC and 0.392% from the analysis. The comparison of the strain between measurement and finite element analysis show that values of the largest strains are 0.7 and 1.5% different in ϵ_{xx} and ϵ_{yy}, respectively. The results confirm that the measured strain field is in good agreement with analysis strain field.

The measured strain from DIC is the total strain, which cannot be used to calculate the stress field. The mechanical strain can be obtained from Eq. 3, and the stress field can be obtained from Eq. 6 using the mechanical strain and the material properties.

$$\epsilon^{\mathbf{M}} = \epsilon^{\text{total}} - \epsilon^{\text{thermal}} \tag{3}$$

$$\epsilon^{\text{thermal}} = \begin{bmatrix} \alpha\Delta T \\ \alpha\Delta T \\ 0 \end{bmatrix} \tag{4}$$

$$\epsilon^{\text{M}} = \begin{bmatrix} \epsilon_{xx}^{\text{total}} - \alpha\Delta T \\ \epsilon_{yy}^{\text{total}} - \alpha\Delta T \\ 2\epsilon_{xy}^{\text{total}} \end{bmatrix} \tag{5}$$

$$\begin{Bmatrix} \sigma_{xx} \\ \sigma_{yy} \\ \sigma_{xy} \end{Bmatrix} = \begin{bmatrix} \frac{E}{1-\nu^2} & \frac{\nu E}{1-\nu^2} & 0 \\ \frac{\nu E}{1-\nu^2} & \frac{E}{1-\nu^2} & 0 \\ 0 & 0 & G \end{bmatrix} \begin{Bmatrix} \epsilon_{xx}^{\text{M}} \\ \epsilon_{yy}^{\text{M}} \\ 2\epsilon_{xy}^{\text{M}} \end{Bmatrix} \tag{6}$$

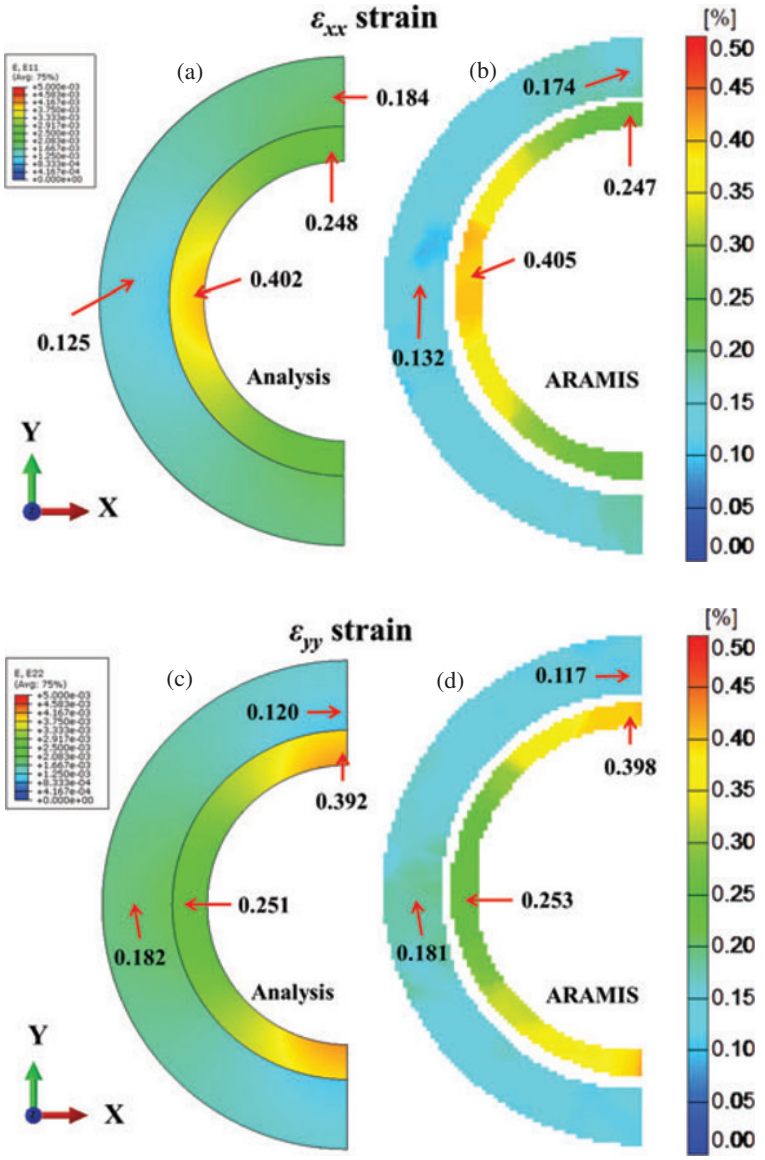

Figure 9 Total strain field calculated by analysis and measured by ARAMIS system of the double ring structure at 200°C. Contours range from 0 to 0.5%. (unit: %)

where ϵ^{M} is the mechanical strain, ϵ^{total} is the total strain, and $\epsilon^{thermal}$ is the thermal strain in Eq. 5. The thermal strains of the aluminum ring and titanium ring are 0.365 and 0.143% under the free boundary condition at 200°C, respectively. The elastic modulus, Poisson's ratio, and shear modulus are denoted by E, ν, and G, respectively. Stress field σ is obtained by using the relationship between strain and stress. Finally, Eqs (3)–(6) were implemented as a script file in the ARAMIS system to calculate the thermal stress of the double ring structure. The errors in strain data should be filtered using a median filter before calculating the stress.

Figure 10 shows the comparisons of the stress fields measured by the ARAMIS system with that calculated from the analysis at 200°C. The location and value of the smallest stress were found to be in good agreement between the ARAMIS system and the analysis. The minimum stress of σ_{xx} is −79.95 MPa from the DIC and −82.82 MPa from the analysis at the top and bottom of the inner ring. Similarly, the minimum stress of σ_{yy} is −83.99 MPa from the DIC and −81.29 MPa from the analysis at the middle of the inner ring.

For a ring structure, stress and strain fields are more useful in the cylindrical coordinates than in Cartesian coordinates. If σ_{xx}, σ_{yy}, and σ_{xy} are the stresses in the orthogonal coordinates, the transformation laws for these stresses between the cylindrical and rectangular Cartesian coordinates can be expressed

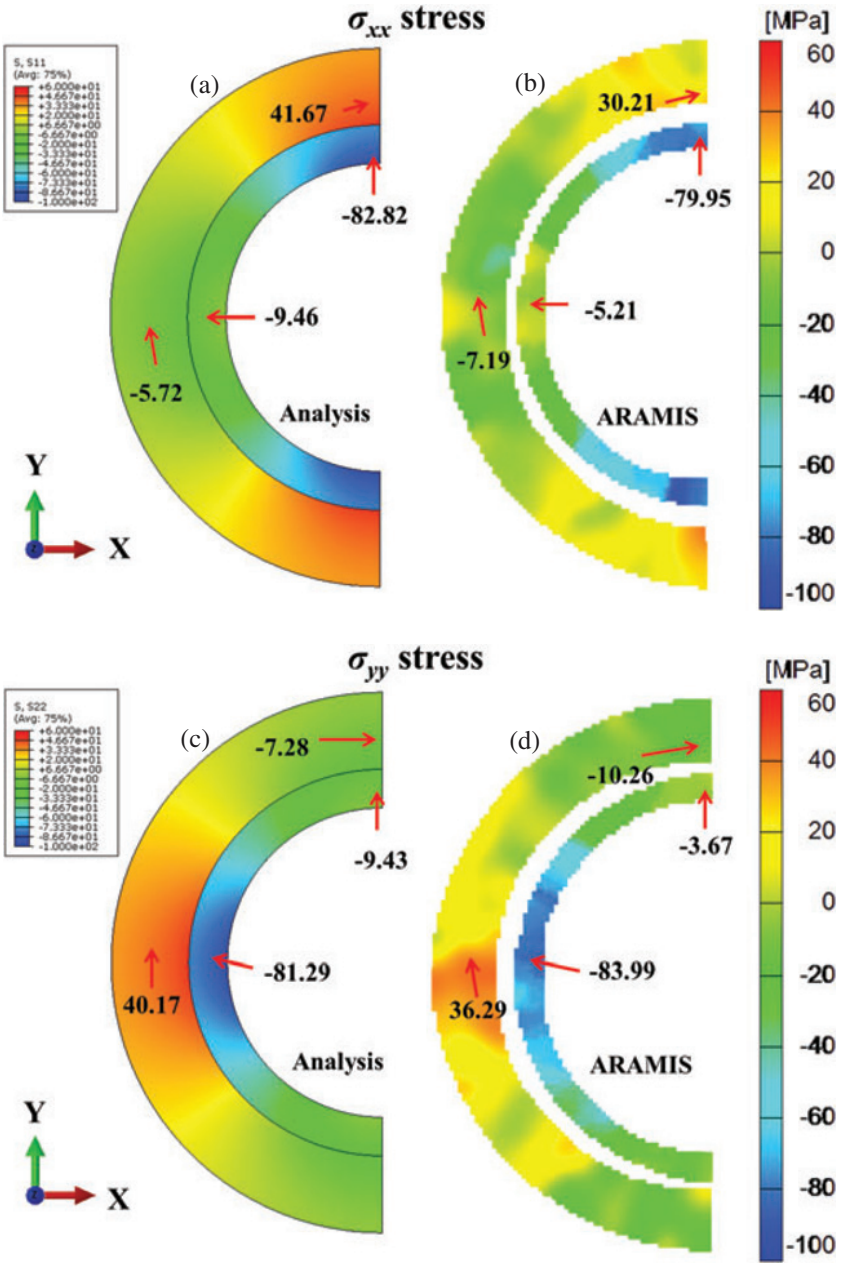

Figure 10 Stress fields calculated by analysis and measured by ARAMIS system for double ring structure at 200°C. Contours range from −100 to 60 MPa. (unit: MPa)

by the following equation:[31]

$$\begin{Bmatrix} \sigma_{rr} \\ \sigma_{\theta\theta} \\ \sigma_{r\theta} \end{Bmatrix} = T \begin{Bmatrix} \sigma_{xx} \\ \sigma_{yy} \\ \sigma_{xy} \end{Bmatrix} = \begin{bmatrix} \cos^2\theta & \sin^2\theta & 2\sin\theta\cos\theta \\ \sin^2\theta & \cos^2\theta & -2\sin\theta\cos\theta \\ -\sin\theta\cos\theta & \sin\theta\cos\theta & \cos^2\theta - \sin^2\theta \end{bmatrix} \times \begin{Bmatrix} \sigma_{xx} \\ \sigma_{yy} \\ \sigma_{xy} \end{Bmatrix} \quad (7)$$

where $\boldsymbol{T}$ is the transformation function, σ_{rr}, $\sigma_{\theta\theta}$, and $\sigma_{r\theta}$ are the stresses expressed in cylindrical coordinates. By applying this equation as an algorithm in the ARAMIS system, the stress can be obtained in cylindrical coordinates.

Figure 11 shows the σ_{rr} stress fields measured by the ARAMIS system and calculated from analysis at 200°C. The σ_{rr} stress field shows negative stress, which means that the inner ring and the outer ring were in compression. The minimum stress was −15.09 MPa at the contact region and the maximum stress was −0.24 MPa at outer of the outer ring. The

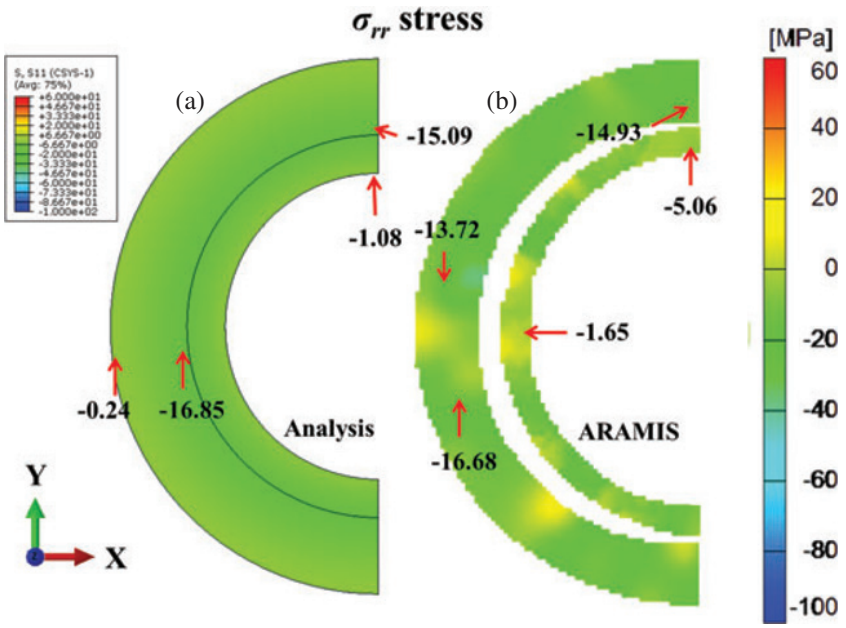

Figure 11 Stress fields calculated by analysis and measured by ARAMIS system for double ring structure at 200°C. Contours range from −100 to 60 MPa. (unit: MPa)

stress measured by DIC showed similar to the stress from analysis, ranging from −1.65 MPa to −16.68 MPa. Although, most of the stress fields measured by ARAMIS system were in good agreement with the stress fields calculated by analysis, several parts showed a big difference, as in Figure 11(b). High concentration stress, which was measured by the ARAMIS system, still remained at the outer edge of the outer ring even though the smoothing process had been applied, as shown in Figure 11(b). The reason for this discrepancy is under investigation.

Conclusion

In this work, the stress measurement method for a structure consisting of more than two kinds of materials was presented. The displacement result from the DIC was in good agreement with the numerical result, showing only several micrometers difference. The algorithm of rigid body elimination in 3D-DIC calculated displacement accurately. Although, the strain and stress fields showed some difference in several parts of the structure, the DIC was able to measure thermal strain and stress. Furthermore, in the future, the averaging methods need to be improved to reduce the error from the differential process. In order to minimize the measurement error, the effects of the image acquisition system and out-of-plane motion need to be reduced. The results in this study indicate that the measurement method, DIC is capable of measuring full-fields stress distributions of the complex structures.

Acknowledgment

This work was supported by the DAPA Defense Acquisition Program Administration and Agency for Defense Development of Republic of Korea. We are very grateful for the fanatical support received.

References

1. Earl, A.T., *Thermal Structures for Aerospace Applications, American Institute of Aeronautics and Astronautics*, Reston, VA (1996).
2. Micro-measurements, *Strain Gauge Selection: Criteria, Procedures, Recommendations*, Tech Note TN-505-4 (2010).
3. Anwander, M., Zagar, B.G., Weiss, B., and Weiss, H., ''Noncontacting Strain Measurements at High Temperatures by the Digital Laser Speckle Correlation,'' *Experimental Mechanics* **40**: 98–105 (2000).
4. Post, D., and Wood, J., ''Determination of Thermal Strains by Moiré Interferometry,'' *Experimental Mechanics* **29**: 318–322 (1989).
5. Han, B., ''Recent Advancements of Moiré and Microscopic Moiré Interferometry for Thermal Deformation Analyses of Microelectronics Devices,'' *Experimental Mechanics* **38**: 278–288 (1998).
6. Lockberg, O.J., Malmo, J.T., and Slettemoen, G.A., ''Interferometric Measurement of High Temperature Objects by Electronic Speckle Pattern Interferometry,'' *Applied Optics* **24**: 3167–3172 (1985).

7. Zandman, F., Redner, S.S., and Post, D., ''Photoelastic-Coating Analysis in Thermal Fields,'' *Experimental Mechanics* **3**: 215–221 (1963).
8. Sutton, M.A., Wolaters, W.J., Peters, W.H., Ranson, W.F., and McNeill, S.R., ''Determination of Displacements Using an Improved Digital Correlation Method,'' *Computer Vision* **1**: 133–139 (1983).
9. Sutton, M.A., Cheng, M., Peters, W.H., Chao, Y.J., and NcNeill, S.R., ''Application of an Optimized Digital Correlation Method to Planar Deformation Analysis,'' *Image and Vision Computing* **4**: 143–150 (1986).
10. Pan, B., Wu, D., and Xia, Y., ''High-Temperature Deformation Field Measurement by Combining Transient Aerodynamic Heating Simulation System and Reliability-Guided Digital Image Correlation,'' *Optics and Lasers in Engineering* **48**: 841–848 (2010).
11. Park, S.B., Dhakal, D., Lehman, L., and Cotts, E., ''Measurement of Deformation in SnAgCu Solder Interconnects Under In Situ Thermal Loading,'' *Acta Materialia* **55**: 3253–3260 (2007).
12. Peter, W.H., and Ranson, W.F., ''Digital Imaging Techniques in Experimental Stress Analysis,'' *Optical Engineering* **21**: 427–432 (1982).
13. Sutton, M.A., Orteu, J.J., and Schreier, H.W., Image Correlation for Shape, Motion and Deformation Measurement, Springer Science and Business Media, New York, NY (2009).
14. Schmidt, T., Tyson, J., and Galanulis, K., ''Full-Field Dynamic Displacement and Strain Measurement Using Advanced 3D Image Correlation Photogrammetry: Part 1,'' *Experimental Techniques* **27**: 47–50 (2003).
15. Yoneyama, S., Kitagawa, A., Lwata, S., Tani, K., and Kikuta, H., ''Bridge Deflection Measurement Using Digital Image Correlation,'' *Experimental Techniques* **31**: 34–40 (2007).
16. Chrysochoos, A., Huon, V., Jourdan, F., Muracciole, J.M., Peyroux, R., and Wattrisse, B., ''Use of Full-Field Digital Image Correlation and Infrared Therography Measurement for the Thermomechanical Analysis of Material Behavior,'' *Strain* **46**: 117–130 (2009).
17. Horacio, D.E., Allison, L.J., Felix, J.L., Owen, Y.L., David, G., and Pablo, D.Z., ''Tablet-Level Origin of Toughening in Abalone Shells and Translation to Synthetic Composite Materials,'' *Nature Communications* **173**: 1–9 (2011).
18. Ha, N.S., JIN, T.L., Goo, N.S., and Park, H.C., ''Anisotropy and Non-Homogeneity of an Allomyrina Dichotoma Beetle Hind Wing Membrane,'' *Bioinspiration & Biomimetics* **6**: 1–15 (2011).
19. Lyons, J.S., Liu, J., and Sutton, M.A., ''High-Temperature Deformation Measurements Using Digital Image Correlation,'' *Experimental Mechanics* **36**: 64–70 (1996).
20. Thompson, R.J., and Hemker, K.J., ''Thermal Expansion Measurement on Coating Materials by Digital Image Correlation,'' *SEM Annual Conference & Exposition on Experimental and Applied Mechanics*, 2007.
21. Pan, B., Wu, D., Wang, Z., and Xia, Y., ''High-Temperature Digital Image Correlation Method for Full-Field Deformation Measurement at 1200°C,'' *Measurement Science and Technology* **22**: 1–11 (2011).
22. Pan, B., Wu, D., and Xia, Y., ''An Active Imaging Digital Image Correlation Method for Deformation Measurement Insensitive to Ambient Light,'' *Optics & Laser Technology* **44**: 204–209 (2012).
23. Sutton, M.A., Yan, J.H., Tiwari, V., Schreier, H.W., and Orteu, J.J., ''The Effect of Out-of-Plane Motion on 2D and 3D Digital Image Correlation Measurements,'' *Optics and Lasers in Engineering* **46**: 746–757 (2008).
24. Lou, P.F., Chao, Y.J., and Sutton, M.A., ''Application of Stereo Vision to 3-D Deformation Analysis in Fracture Experiments,'' *Optical Engineering* **33**: 981–990 (1994).
25. Lou, P.F., Chao, Y.J., Sutton, M.A., and Peters, W.H., ''Accurate Measurement of Three-Dimensional Deformations in Deformable and Rigid Bodies Using Computer Vision,'' *Experimental Mechanics* **33**: 123–132 (1993).
26. Faugeras, O., *Three-Dimensional Computer Vision: A Geometric Viewpoint*, MIT Press, London, UK. (1993).
27. Helm, J.D., McNeill, S.R., and Sutton, M.A., ''Improved 3-D Image Correlation for Surface Displacement Measurement,'' *Optical Engineering* **35**: 1911–1920 (1996).
28. Langford, M.J., Fox, A., and Smith, R.S., *Langford's Basic Photography*, 9th Edition, Focal Press, New York, NY (2010).
29. *ARAMIS. v.6.0.2 User's Manual Revision A*. GOM mbH, Braunschweig (2007).
30. U.S. Department of Transportation, *Metallic Materials Properties Development and Standardization*, Office of Aviation Research, Washington, D.C. (2003).
31. Saouma, V.E., *Introduction to Continuum Mechanics and Elements of Elasticity/Structural Mechanics*, Department of Civil Environmental and Architectural Engineering, University of Colorado, Boulder, CO (1998).